Earthquake Geotechnical Engineering for Protection and Development of Environment and Constructions – Silvestri & Moraci (Eds)
© 2019 Associazione Geotecnica Italiana, Rome, Italy, ISBN 978-0-367-14328-2

A bounding surface plasticity model for normally consolidated volcanic cohesive soils subjected to cyclic loading

X.S. Kang
State Key Laboratory for Strength and Vibration of Mechanical Structures, School of Aerospace Engineering, Xi'an Jiaotong University, Xi'an, Shaanxi, China

J.H. Zhang
Department of Civil Engineering, Xi'an Jiaotong University, Xi'an, Shaanxi, China

C.M. Ning
Campus Planning and Basic Construction Management Center, Xi'an Jiaotong University, Xi'an, Shaanxi, China

H.J. Liao*
Department of Civil Engineering, Xi'an Jiaotong University, Xi'an, Shaanxi, China

ABSTRACT: A new plastic modulus is proposed by introducing three new parameters, which control the stress paths of volcanic cohesive soils subjected to cyclic loading. Then, a bounding surface plasticity model is formulated by introducing the new plastic modulus, a structural bounding surface, a loading surface, a mapping rule and a plastic potential. Comparisons between the model simulation and experimental data show that the model can capture the pore pressure and stress path of normally consolidated volcanic cohesive soils subjected to cyclic loading.

KEY WORDS: Bounding plasticity theory; cyclic loading; volcanic cohesive soils; normally consolidated; plastic modulus

1 INTRODUCTION

Stress-strain relationship and stress path of volcanic cohesive soils has been studied via monotonic loading test (Liao 1996; Kiyohara & Kazama 2014) and cyclic loading test (Liao 1996; Liao 1998). To our knowledge, the existing constitutive models for simulating the cyclic behavior mainly focus on sands (Khalili et al. 2005; Kan et al. 2014; Taiebat & Dafalias 2008; Dafalias & Taiebat 2016), clay (Li et al. 2016; Zhang et al. 2015) and brittle rock (Cerfontaine et al. 2017).

For sands, Khalili et al. (2005) formulated a constitutive model by introducing a mapping rule. To avoid the complexity of the mapping rule, Kan et al. (2014) developed the constitutive model by introducing a simplified mapping rule. However, the two models mainly focus on simulating the drained cyclic test on sand, not the undrained cyclic test on sand. Dafalias & Taiebat (2016) formulated a developed constitutive model based on an anisotropic sand constitutive model (Taiebat & Dafalias 2008). In the model, the yield surface shrinks to zero, and the plastic loading occurs for any direction of the stress ratio. For clay, Li et al. (2016) derived an implicit integration of a model by introducing a popular return mapping algorithm. The corresponding algorithm is stable and accurate, which has been verified by the comparison between tests and simulations. Different from the traditional elasto-plastic models, Zhang et al. (2015) established a constitutive model for clay that does not require a yield surface and a flow rule. The model is formulated via a quantitative description of the energy in the

reversible and irreversible processes. For brittle rock, Cerfontaine et al. (2017) formulated a constitutive model for describing the cyclic behavior at low confinement. The above constitutive models indicate that the bounding surface plasticity theory can be used for formulating constitutive models to simulate the cyclic behavior. However, the bounding surface theory has not been used for normally consolidated volcanic cohesive soils subjected to cyclic loading.

The aim of the paper is to develop a constitutive model for normally consolidated volcanic cohesive soils subjected to cyclic loading. Firstly, we propose a new plastic modulus that is used for the cyclic loading of the volcanic cohesive soils. Secondly, we formulate a bounding surface plasticity model for the volcanic cohesive soils by introducing a structural bounding surface, loading surface, mapping rule, plastic potential function and the plastic modulus. Finally, we verify the new plastic modulus using a cyclic loading test on volcanic cohesive soils.

2 BOUNDING SURFACE PLASTICITY

The bounding surface plasticity includes a bounding surface, a loading surface, a mapping rule and a plastic potential (Dafalias 1986). A current stress $\boldsymbol{\sigma}'$ locates on the loading surface f. An image stress $\bar{\sigma}'$ locates on the bounding surface $\bar{f}$. The plastic potential surface is g. These surfaces can be written as follows:

$$\begin{cases} f(\boldsymbol{\sigma}', \sigma_n) = 0 \\ \bar{f}(\bar{\boldsymbol{\sigma}}', \bar{\sigma}_n) = 0 \\ g(\boldsymbol{\sigma}', \sigma_0) = 0 \end{cases} \tag{1}$$

where σ_n, $\bar{\sigma}_n$ and σ_0 controls the size of the loading surface, the bounding surface and the plastic potential surface, respectively.

2.1 *Bounding surface*

Kang and Liao (2019) used a structural bounding surface to predict stress-strain relationship and stress paths. In the surface, $M(\theta)$ equals to M_c for triaxial compression condition (θ=0°); $M(\theta)$ equals to M_e for traxial extension condition (θ=60°). To predict the stress paths of volcanic cohesive soils under cyclic loading test, the structural bounding surface is adopted:

$$\bar{f} = \bar{q}^2 - {M_\alpha}^2(\bar{p}' + p_s')(\bar{p}_0' - \bar{p}') = 0 \tag{2}$$

where $(\bar{p}', \bar{q})$ is the image stress, p_s' is the structural strength, $\bar{p}_0'$ controls the size of the structural bounding surface, and M_α is the slope of the critical state line. M_α equals M_c and M_e for triaxial compression condition and traxial extension condition, respectively. The image stress $(\bar{p}', \bar{q})$ is calculated by using a mapping rule.

The unit normal vector that is perpendicular to the bounding surface is given by:

$$\boldsymbol{n} = (n_p, n_q)^T \tag{3}$$

The partial derivatives in Eq. (3) are shown in Appendix A.

$\dot{p}_s'$ and $\bar{\sigma}'$ used by Kang and Liao (2019) are adopted:

$$\dot{p}_s' = -\dot{\varepsilon}_q^p p_s'/\varepsilon_{ref} \tag{4}$$

$$\dot{\bar{p}}_0' = C_p \bar{p}_0' \dot{\varepsilon}_p^p - p_s' \dot{\varepsilon}_q^p/\varepsilon_{ref} \tag{5}$$

where $\dot{\varepsilon}_q^p$ and $\dot{\varepsilon}_p^p$ are the increments of the plastic shear strain and plastic volumetric strain, respectively. ε_{ref} is a reference strain. C_p represents $(1 + e_0)/\lambda - \kappa$.

2.2 *Loading surface and mapping rule*

Being similar to the structural bounding surface, the loading surface is given by:

$$f(p', q, p'_s, \bar{p}'_0) = q^2 - M_\alpha{}^2(p' + p'_s)(p'_0 - p') = 0 \tag{6}$$

where (p', q) is the current stress, which always lies on the loading surface. The shape of the loading surface in the meridional plane is shown in Figure 1. In Eq. (6), $p' = \sigma_{ii}/3$ and $q = \sqrt{3/2 s_{ij} s_{ij}}$.

A simplified mapping rule proposed by Kan et al. (2014) is adopted, although some other mapping rules are efficient in describing cyclic loading (Taiebat & Dafalias 2010; Dafalias & Taiebat 2016; Li 2016). For the first loading condition (see Figure 1), the original point is defined as the projection center. For unloading and reloading condition (see Figure 2), the projection center is the center of similarity, which moves to the last point of stress reversal. The point of stress reversal is determined if $n : \dot{\sigma}' < 0$. Then, a new loading surface is expanding as compressive or extensive loading, as shown in Figure 2.

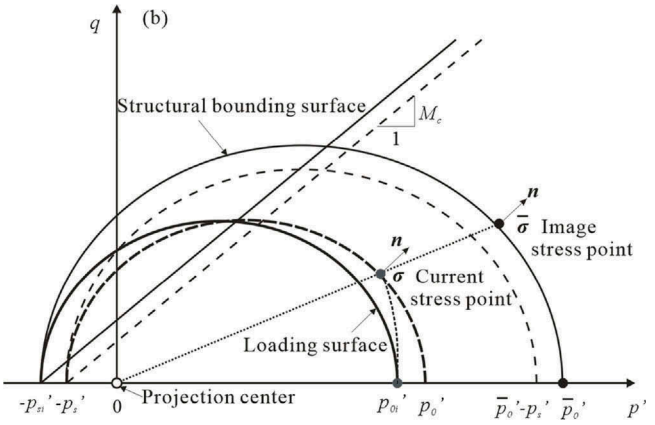

Figure 1. Bounding surfaces and loading surfaces in the meridional plane.

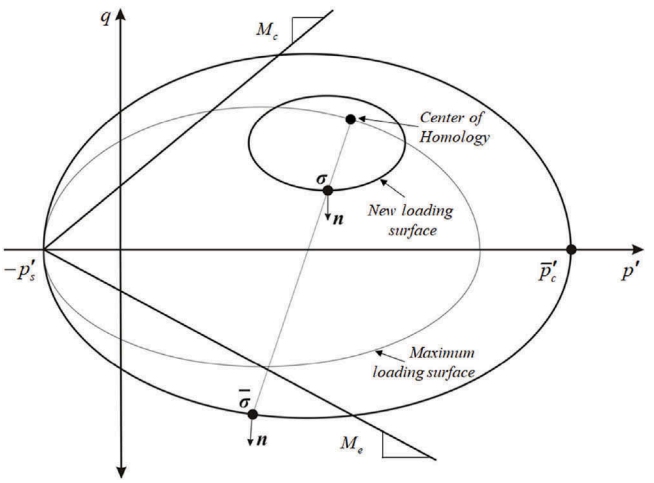

Figure 2. Mapping rule for expressive loading and compressive loading.

2.3 *Plastic potential surface*

Noting the plastic potential function of the Cam-clay model (Roscoe et al. 1963), a simple plastic potential function for cyclic loading is defined as:

$$g = tq + M_d p' \ln(p'/p'_0)) \tag{7}$$

where M_d is a parameter that determines a state that corresponds to the $\dot{\varepsilon}_v$=0. p'_0 controls the size of the plastic potential surface. The value of t is determined by the image deviatoric stress $\bar{q}$, according to a model proposed by Khalili et al. (2005). t=+1 for compressive loading ($\bar{q}$>0) and t=-1 for extensive loading ($\bar{q}$<0), as shown in Figure 3. This enable the plastic volumetric strain to avoid sudden change at q=0.

The unit normal vector that is perpendicular to the plastic potential surface is given by:

$$\boldsymbol{m} = [m_p, m_q]^T \tag{8}$$

where m_p and m_q are shown in Appendix A.

2.4 *A new plastic modulus*

According to the bounding surface plasticity (Dafalias 1986), the total plastic modulus includes two parts:

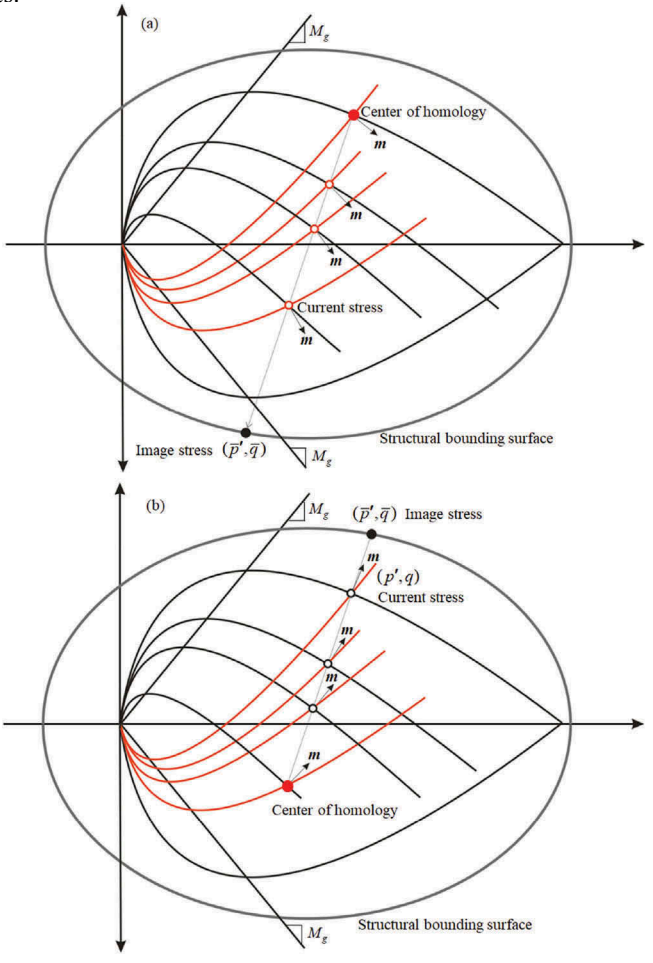

Figure 3. Plastic flow vector during (a) extensive loading ($\bar{q}$<0) and (b) compressive loading ($\bar{q}$>0).

$$H=H_b+H_f \tag{9}$$

where H_b is the plastic modulus that is determined by the image stress $\bar{\sigma}'$, H_f is the plastic modulus that is related to the "distance" between σ' and $\bar{\sigma}'$.

Substituting Eq. (A9), Eq. (A10), Eq. (A11) and Eq. (A12) into Eq. (B4), the plastic modulus H_b is derived:

$$H_b = M_\alpha{}^2 C_p \bar{p}'_0(\bar{p}' + p'_s)(M_d - t\eta) - M_\alpha{}^2 t(\bar{p}'_0 + p'_s)p'_s/\varepsilon_{ref} \tag{10}$$

To describe the cyclic behaviour of volcanic cohesive soils, a new expression of plastic modulus H_f is defined as follows:

$$h_f = h_{bi}^{\alpha}(\bar{p}'_0/p'_0 - 1)^{0.2}(M - \beta t\eta) \tag{11}$$

$$\alpha=\begin{cases} \alpha_1 & T<T_0 \\ \alpha_2 + (\alpha_1 - \alpha_2)\sqrt{T_0/T} & TT_0 \end{cases} \tag{12}$$

where α_1 andα_2 are parameters that control the loose of the hysteresis loop (α_1>α_2), as shown in *Figure 4*. α_1 increases as the slope of stress paths before the critical state. α_2 increases as the width of hysteresis loops near the critical state. β is related to the accumulation of plastic shear strain. h_{bi} is the initial values of the plastic modulus h_b. T_0 is on the threshold of critical state, which equals $2N_{ref}\pi/\Delta$. N_{ref} is the numbers of the hysteresis loop before the critical state. Δ equals $2\pi/100$.

2.5 *Stress-strain relationship*

The incremental form of the stress-strain relationship is:

$$\dot{\boldsymbol{\sigma}}' = \left(\boldsymbol{D}^e - \frac{\boldsymbol{D}^e \boldsymbol{m}\boldsymbol{n}^T \boldsymbol{D}^e}{H/l_g l_{\bar{f}} + \boldsymbol{n}^T \boldsymbol{D}^e \boldsymbol{m}} \right) \dot{\boldsymbol{\varepsilon}} \tag{13}$$

where m is the unit normal vector that is perpendicular to the plastic potential surface g, n is the unit vector that is perpendicular to the bounding surface $\bar{f}$, D is the elastic matrix, H is the total plastic modulus. K and G are determined by $(1+ e_0)p'/\kappa$ and $3K(1\text{-}2\mu)/(2(1+\mu))$, respectively (Roscoe et al. 1963).

3 MODEL CALIBRATION AND VALIDATION

3.1 *Model calibration*

λ, κ, M_α, M_d, ε_{ref}, μ and e_0 are general parameters. λ and κ are determined via isotropic consolidation tests. M_α is obtained from triaxial compression and extension test. M_d is equal to $0.85M_\alpha$. μ is assumed to be 0.3. e_0 is the void ratio at p'=150kPa. ε_{ref} is assumed to be 0.03, which is determined via trial and error method.

α_1, α_2, N_{ref} and β are determined directly from cyclic loading test. The values of N_{ref} are the numbers of hysteresis loops before the critical state. α_1 and α_2 present the slope of the initial and final stress path, respectively. The values of α_1 and α_2 are determined via trial and error method. β is related to the accumulation of plastic shear strain. The model parameters for the volcanic cohesive soils are shown in Table 1.

Table 1. Model parameters for the volcanic cohesive soils.

M_c	M_e	μ	e_0	ε_{ref}	λ	κ	N_{ref}	α_1	α_2	β
1.59	1.34	0.3	3.085	0.03	0.212	0.034	4	1.55	0.80	0.75

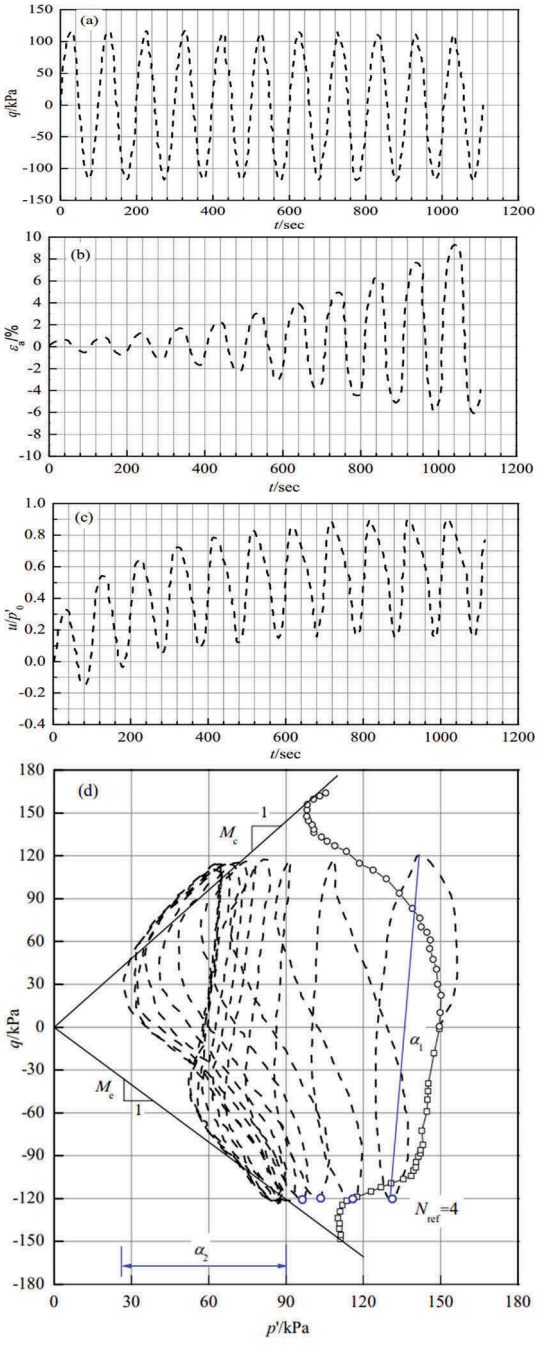

Figure 4. Undrained cyclic loading test on normally consolidated volcanic cohesive soils. (after Liao 1996)

3.2 *Model validation*

The model was verified by cyclic loading tests on volcanic cohesive soils (Liao 1996). Figure 4 shows the experimental data of undrained cyclic test on the volcanic cohesive soils. Figure 5 shows the model simulation for undrained cyclic test on the volcanic cohesive soils. Comparison between experimental data and model simulation shows that the pore pressure and critical state can be captured by the model. But the axial strain is not well captured by the proposed model.

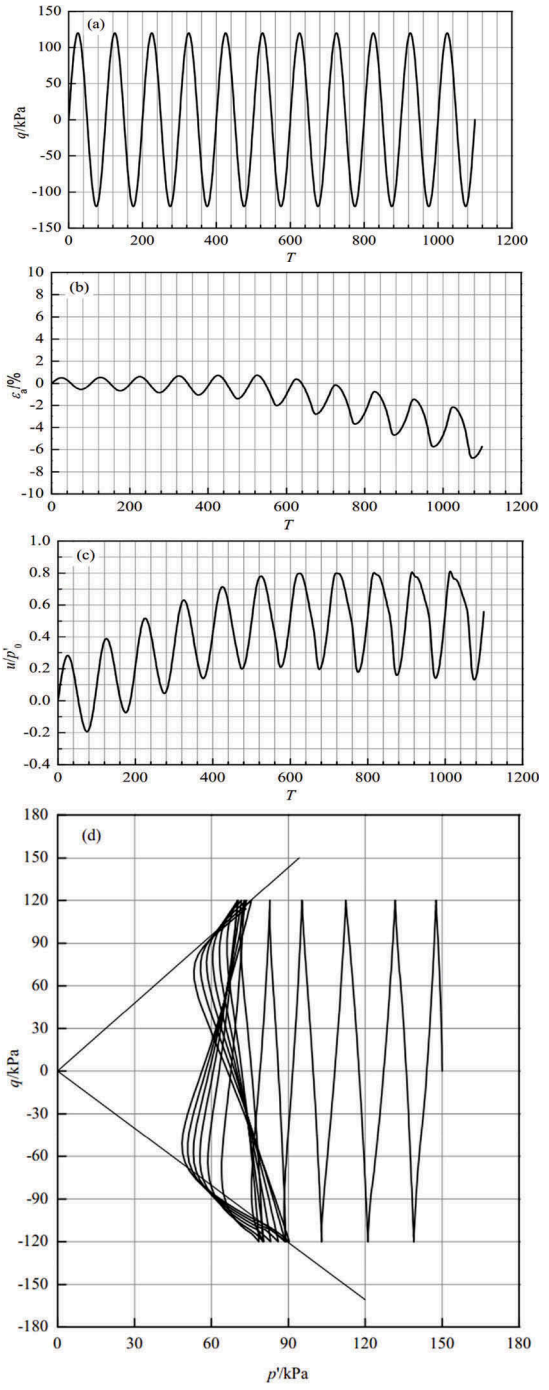

Figure 5. Model simulation for undrained cyclic loading test on volcanic cohesive soils.

4 CONCLUSION

A bounding surface plasticity model is formulated for volcanic cohesive soils subjected to cyclic loading, based on the bounding surface plasticity theory. In the model, a new expression of plastic modulus is proposed for cyclic loading by introducing three new parameters. The model has been verified by the cyclic loading tests on volcanic cohesive soils. Comparison between experimental

data and model simulation shows that the pore pressure and stress paths agree with the experimental data. The axial strain of volcanic cohesive soils can't be well captured by the model.

ACKNOWLEDGEMENTS

The authors wish to thank the financial support provided by the Natural Science Foundation of China (51879212, 41630639), the Open Research Fund of State Key Laboratory of Geomechanics and Geotechnical Engineering, the Institute of Rock and Soil Mechanics, Chinese Academy of Science (Z016008) and the Opening Research Foundation of Key Laboratory of Western Mineral Resources and Geological Engineering Ministry of Education (310826171107).

REFERENCES

Dafalias, Y.F. 1986. Bounding surface plasticity. I: Mathematical foundation and hypoplasticity. *Journal of Engineering Mechanics* 112(9): 966-987.

Dafalias, Y.F. & Taiebat, M. 2016. SANISAND-Z: zero elastic range sand plasticity model. *Géotechnique* 66(12):1-15.

Khalili, N., Habte, M.A. & Valliappan, S. 2005. A bounding surface plasticity model for cyclic loading of granular soils. *International Journal for Numerical Methods in Engineering* 63(14):1939-1960.

Kan, M.E., Taiebat, H.A. & Khalili, N. 2014. Simplified mapping rule for bounding surface simulation of complex loading paths in granular materials. *International Journal of Geomechanics* 14(2):239-253.

Kiyohara, Y. & Kazama, M. 2014. Shearing behavior and modeling of disturbed volcanic cohesive soil considering dependence of hydraulic hysteresis on void ratio. In Sydney, Australia, *6th International Conference on Unsaturated Soils*; Proc. intern. symp., Sydney,2-4 July 2014.

Kikumoto, M., Nguyen, V.P.Q., Yasuhara, H. & Kishida, K. 2017. Constitutive model for soft rocks considering structural healing and decay. *Computers & Geotechnics* 91:93-103.

Kang XS, Liao HJ. 2019. Bounding surface plasticity model for jointed soft rocks considering overconsolidation and structural decay. *Computers and Geotechnics* 108:295-307.

Liao, H.J. 1996. A Foundation study on strength-deformation characteristics of soft rock and cohesive soil, Ph.D. Thesis, Tokai University, Japan.

Liao, H.J., Yu, M.H., Akira Tonosaki, et al. 1998. Dynamic shear strength of Loessial Soils and Volcanic cohesive Soils. *Journal of Xi'an Jiaotong Univerisity* 32(10): 70-74. (in Chinese)

Liao, H.J., Su, L.J., Pu, W.C. & Yin, J.H. 2003. Test and numerical analysis of the constitutive relation of a diatomaceous soft rock. *Marine Georesources & Geotechnology* 21(3-4):183-200.

LI, J. 2016. On implicit integration of the bounding surface model based on swell–shrink rules. *Applied Mathematical Modelling* 40:8671-8684.

Roscoe, K.H. & Schofield, A.N. 1963. Thurairajah A. Yielding of clays in states wetter than critical. *Géotechnique* 8(2):22-53.

Taiebat, M. & Dafalias, Y.F. 2010. SANISAND: Simple anisotropic sand plasticity model. *International Journal for Numerical & Analytical Methods in Geomechanics* 32(8):915-948.

Zhang, Z. & Cheng, X. 2015. A thermodynamic constitutive model for undrained monotonic and cyclic shear behavior of saturated soils. *Acta Geotechnica* 10(6):1-16.

APPENDIX A

$$n_p = \frac{\partial \bar{f}}{\partial \bar{p}'} \frac{1}{l_{\bar{f}}} \tag{A1}$$

$$n_q = \frac{\partial \bar{f}}{\partial \bar{q}} \frac{1}{l_{\bar{f}}} \tag{A2}$$

$$m_p = \frac{\partial g}{\partial p'} \frac{1}{l_g} \tag{A3}$$

$$m_p = \frac{\partial g}{\partial q}\frac{1}{l_g} \tag{A4}$$

$$l_g = \sqrt{\left(\frac{\partial g}{\partial p'}\right)^2 + \left(\frac{\partial g}{\partial q}\right)^2} \tag{A5}$$

$$l_{\bar{f}} = \sqrt{\left(\frac{\partial \bar{f}}{\partial \bar{p}'}\right)^2 + \left(\frac{\partial \bar{f}}{\partial \bar{q}}\right)^2} \tag{A6}$$

$$\frac{\partial \bar{f}}{\partial \bar{p}'} = M_\alpha{}^2(2\bar{p}' - \bar{p}'_0 + p'_s) \tag{A7}$$

$$\frac{\partial \bar{f}}{\partial \bar{q}} = 2\bar{q} \tag{A8}$$

$$\frac{\partial \bar{f}}{\partial \bar{p}'_0} = -M_\alpha{}^2(\bar{p}' + p'_s) \tag{A9}$$

$$\frac{\partial \bar{f}}{\partial p'_s} = M_\alpha{}^2(\bar{p}' - \bar{p}'_0) \tag{A10}$$

$$\frac{\partial g}{\partial p'} = M_d - t\eta \tag{A11}$$

$$\frac{\partial g}{\partial q} = t \tag{A12}$$

APPENDIX B

The differential form of the structural bounding surface is:

$$\dot{\bar{f}} = \frac{\partial \bar{f}}{\partial \bar{p}'}\dot{\bar{p}}' + \frac{\partial \bar{f}}{\partial \bar{q}}\dot{\bar{q}} + \frac{\partial \bar{f}}{\partial \bar{p}'_0}\dot{\bar{p}}'_0 + \frac{\partial \bar{f}}{\partial p'_s}\dot{p}'_s = 0 \tag{B1}$$

Substituting Eqs. (5) and (6) into Eq. (B1):

$$\frac{\partial \bar{f}}{\partial \bar{p}'}\dot{\bar{p}}' + \frac{\partial \bar{f}}{\partial \bar{q}}\dot{\bar{q}} + \frac{\partial \bar{f}}{\partial \bar{p}'_0}\left(C_p\bar{p}'_0\dot{\varepsilon}^p_p - \frac{1}{\varepsilon_{ref}}p'_s\dot{\varepsilon}^p_q\right) + \frac{\partial \bar{f}}{\partial \bar{p}'_s}\left(-\frac{1}{\varepsilon_{ref}}p'_s\dot{\varepsilon}^p_q\right) = 0 \tag{B2}$$

Substituting $d\varepsilon^p_p = \dot{\Lambda}\partial g/\partial p'$ and $d\varepsilon^p_p = \dot{\Lambda}\partial g/\partial q$ into Eq. (B2), the plastic multiplier $\dot{\Lambda}$ is obtained as:

$$\dot{\Lambda} = \frac{\frac{\partial \bar{f}}{\partial \bar{p}'}\dot{\bar{p}}' + \frac{\partial \bar{f}}{\partial \bar{q}}\dot{\bar{q}}}{\left(\frac{\partial \bar{f}}{\partial \bar{p}'_0} + \frac{\partial \bar{f}}{\partial \bar{p}'_s}\right)\frac{1}{\varepsilon_{ref}}\frac{\partial g}{\partial q}p'_s - \frac{\partial \bar{f}}{\partial \bar{p}'_0}C_p\bar{p}'_0\frac{\partial g}{\partial p'}} \tag{B3}$$

The plastic modulus H_b that is related to the image stress $\bar{\sigma}'_{ij}$ is given by:

$$H_b = \left(\frac{\partial \bar{f}}{\partial \bar{p}'_0} + \frac{\partial \bar{f}}{\partial p'_s}\right)\frac{1}{\varepsilon_{ref}}\frac{\partial g}{\partial q}p'_s - \frac{\partial \bar{f}}{\partial \bar{p}'_0}\frac{\partial g}{\partial p'}C_p\bar{p}'_0 \tag{B4}$$